Sol–gel thermal barrier coatings: Optimization of the manufacturing route and durability under cyclic oxidation

Julien Sniezewski [a], Yannick LeMaoult [a], Philippe Lours [a], Lisa Pin [a], Vincent Menvie Bekale [b], Daniel Monceau [b], Djar Oquab [b,*], Justine Fenech [c], Florence Ansart [c], Jean-Pierre Bonino [c]

[a] Université de Toulouse, ICA Mines-Albi, 81013 Albi France, France
[b] Université de Toulouse, Institut Carnot CIRIMAT, ENSIACET, 4 allée Emile Monso, BP-44362, 31030 Toulouse Cedex 4, France
[c] Université de Toulouse Institut Carnot CIRIMAT-UPS, 118, Route de Narbonne, 31062 Toulouse cedex 09, France

A B S T R A C T

A new promising and versatile process based on the sol–gel transformation has been developed to deposit yttria-stabilised thermal barrier coatings. The non-oriented microstructure with randomly structured pore network, resulting from the soft chemical process, is expected to show satisfactory thermo-mechanical behaviour when the TBC is cyclically oxidized. First stage of the research consists of optimizing the processing route to generate homogeneous microstructure and controlled surface roughness. The objective is to reduce, as much as possible, the size and depth of the surface cracks network inherent to the process. Indeed, the durability of the TBC when cyclically oxidized strongly depends on the sharpness of those cracks that concentrate thermo-mechanical stresses and generate detrimental propagation resulting in spallation. Cyclic oxidation tests are performed using a cyclic oxidation rig instrumented with CCD cameras to monitor in a real time basis the mechanism of crack propagation and spallation. The impact of various parameters either directly related to the processing route, e.g. the intimate microstructure of the TBC and the TBC thickness, or to the thermal loading, e.g. the oxidation temperature and the cumulated hot time, on the durability of the TBC is investigated.

Keywords:
Sol–gel
YSZ
Thermal barrier coating
Spallation
Oxidation
High temperature
Rumpling

1. Introduction

Thermal Barrier Coatings (TBCs) are used as insulators on hot section components to reduce operating temperatures in aircraft engines, marine propulsion and industrial gas turbine. At an industrial scale, the Electron Beam Physical Vapour Deposition (EB-PVD) and the Air Plasma Spray (APS) are the two physical processes used in the industry to produce thermal barrier coatings. By these processes, coatings have different microstructures: lamellar microstructure consisting in splats superposition for PS coatings with thermal conductivity in the range from 0.7 to 0.9 $W m^{-1} K^{-1}$ and column-like microstructure for EBPVD coatings with best mechanical performances. However, in this last case, perpendicular orientation of the columns makes that thermal conductivity is twice higher compared to PS coating.

In this paper, we carry out the sol–gel route as an alternative method in order to test a new microstructure. The sol–gel route is a versatile process able to produce either thin ceramic coatings or thick deposits [1–3].

* Corresponding author.
E-mail address: djar.oquab@ensiacet.fr (D. Oquab).

It is based on the transition from a liquid phase (sol) to a solid phase (gel) by a series of hydrolysis and condensation reactions. This soft chemical route allows developing non-oriented microstructure with randomly oriented pore network [4] which is expected to exhibit satisfactory thermomechanical performances. In addition, sol–gel route may offer substantial benefits in terms of process feasibility and cost and possibility of repairing damaged TBC. Sol–gel processing has gained considerable ground and credibility in recent years as alternative methods of thermal or plasma spraying and physical vapour deposition to obtain coatings with non directional porosity. For example, Barrow et al. [5] has developed this technique to prepare films thicker than 10 mm and up to 200 mm by successive coatings. Xia et al. [6] have also used the sol–gel route to develop sols for the colmatation of cracks generated by thermal treatment. But in both cases, the process consists of mixing sols with commercial powders or powders obtained by co-precipitation technique. In our case, the originality is of dispersing the precursor powder into the mother sol, both obtained by the same sol–gel route. The main advantage is that this powder has a very fine granulometry, a monodisperse size distribution and a good affinity with the sol. Furthermore, it is possible to prepare a mixture with multimodal powders to exhibit new microstructures (porosity control, gradient...).

Nevertheless, it is of utmost concern to verify whether the sintered sol–gel TBC thermomechanical and erosion behaviour under thermal

doi:10.1016/j.surfcoat.2010.10.036

loading in cyclic oxidation conditions is appropriate to a proper use in service. In this paper, a novel route to optimise the microstructure of the sol–gel TBC as well as the cyclic oxidation behaviour at both 1100 °C and 1150 °C and the influence of the coating thickness are discussed.

2. Experimental

2.1. Substrate pre-treatment

The β-(Ni,Pt)Al coated first generation AM1® substrates used in the present study were provided by Snecma-SAFRAN (Chatellerault, France). The single phase β-(Ni,Pt)Al bond coat was formed by platinum deposition via an electrolytic process followed by vapour phase aluminization (APVS) and diffusion heat treatment [7]. Because of process requirement, a Hastelloy X stem was welded to the AM1 disc and also entirely covered by the bond coating. The as-received NiPtAl/AM1 substrates were mechanically ground with 600 grit silicon carbide SiC abrasive paper. The mechanical grinding suppresses the roughness due to grain boundaries growth during the aluminization process [8]. So, compared to the initial roughness (Ra ~ 1 μm), the grinding with 600 grit SiC paper results of very low surface roughness Ra of 0.14 μm, as measured by laser interferometer. These ground substrates were then pre-oxidized at 950 °C for 2 h at 5×10^{-4} mbar synthetic air vacuum to favour the formation of a thin alpha alumina layer [7,8]. The obtained oxide scale (TGO) thickness was estimated to be 0.35 μm thick after pre-oxidation, from mass gain measurements. Photo stimulated luminescence spectroscopy (PSLS) measurements allowed identifying some transient gamma and teta alumina in addition to the most stable alpha alumina in the TGO [8].

2.2. Sol–gel deposition process

The YSZ top-coat was deposited on pre-treated substrates by the sol–gel route. The sol was synthesized from zirconium (IV) propoxide ($Zr(OPr)_4$) (Aldrich), yttrium (III) nitrates hexahydrate (Acros Organics) and 1-propanol as solvent. To reduce the zirconium alkoxide reactivity towards water and to avoid hydroxides formation, acetylacetone (AcAc) has been used as complexing agent. The two molar ratio [$AcAc/Zr(OPr)_4$] and [$H_2O/Zr(OPr)_4$] have been kept constant to 0.7 and 8.5 respectively and zirconium propoxide concentration to 0.5 mol l^{-1}. The ratio of starting precursors is calculated in order to obtain a composition of ZrO_2-5 mol% Y_2O_3. At the same time, a slurry was prepared by spreading out an appropriate amount of zirconia powder ZrO_2-8 mol% Y_2O_3 (Tosoh) with submicron particles (40.8 wt.%) in 1-propanol (40.8 wt.%) and some water (2.4 wt.%) in order to achieve the concentration of 800 g l^{-1}. The water addition helped to reduce the amount of large agglomerates (about 50 μm) in comparison with the previous fabrication reported in [8]. To complete homogenization of the mixture, mechanical stirring followed by sonication were applied for optimum time. Then, 20 vol.% of the initially synthesized sol was added to 80 vol.% of the slurry to form the composite sol.

Ceramic layer was prepared by the dip-coating technique i.e. by immersion of the substrates into the composite sol and withdrawn at a controlled speed (250 mm/min). Finally, samples were dried at room temperature and further on, heat treated in static air 2 h at 600 °C (heating rate of 0.8 °C min^{-1}) and 2 h at 950 °C (heating rate of 2.5 °C min^{-1}).

2.3. Cyclic oxidation

Thermal barrier coatings are cyclically oxidised in a rig able to monitor, using various types of optical means, the evolution of the specimen surface during the phases of cooling [9]. Typical cycles include 5 min heating, 1 h holding at high temperature and 5 min cooling down to room temperature. Image analysis is used to derive quantitative data relative to the extent of surface damage. Individual images are first binarized to define a contrast threshold used to discriminate the zones of surface degradation, typically in dark, and the zones where the TBC remained adherent to the substrate, typically in white. Based on geometrical considerations, an algorithm is then used to separate high and low elongated defects corresponding respectively to the cracks and the spalls. Surface fraction of cracks (respectively spalls) corresponds to the ratio between the total surface of cracks (respectively spalls) and the specimen surface calculated by subtracting the surface of an outer ring, 1.5 mm width, to avoid any edge effects.

3. Results of cyclic oxidation and discussion

In direct relation with the processing route, the sol–gel thermal barrier coatings show very specific microstructures. Namely, the intimate structure of the deposit is basically non columnar and mostly equiaxial including a significant density of porosity. The thickness of the barrier depends on the number of dip-coatings and other process parameters such as the rate of withdrawal from the composite sol or the viscosity of the sol. Though higher thicknesses, more than 100 μm, are achievable, the present work will focus on barriers, deposited using the controlled process parameters described in Section 1, with thickness typically ranging from 20 μm to 100 μm. As the final heat treatment of specimen proceeds, the sintering of deposits causes the formation of a regular network of surface cracks, delimitating YSZ cells with size in the range 100 μm to 200 μm. This results from the thermally activated material shrinkage prone to induce bi-axial stresses higher than the stress to rupture of the coatings. The bi-axial nature of the stress leads to the formation of an almost isotropic pattern of individual cells separated by sintering-induced cracks. Providing it is perfectly controlled, in terms of kinetics and morphology, this initial crack network (heat checking) may be beneficial to the further mechanical strength of the barrier while thermally cycled. Indeed, the occurrence of penetrating cracks perpendicular to the specimen surface can significantly enhance the lateral compliance of the deposit as sought, to some extent, in standard EB-PVD TBC or in plasma sprayed TBC as mentioned in [10].

3.1. Cracking, heat-checking and spalling of TBC

Fig. 1 shows images of a coated specimen surface, extracted from the CCD camera video recording of successive cooling phases after high temperature exposure at 1150 °C. Photographs are taken when cooling is fully completed upon return to room temperature, namely after 5, 20, 40 and 55 cycles. The first image at the top left of the figure represents the initial specimen, as deposited and heat-treated, prior to any oxidation cycle. The last image at the bottom right corresponds to the material damaged surface after 55 cycles viewed with oblique lighting. Inserted in each image, are high magnification SEM micrographs showing the detail of the surface damages including cracking and spallation. Up to 20 cumulated cycles, the main damaging effect is the development of the pre-existing cracks either through the formation of additional crack within the cells of the initial network, the closing – through crack propagation – of the existing cells or the widening of the crack themselves as a consequence of further sintering of the TBC.

The onset for spallation requires between 20 and 40 cycles of 1 h at 1150 °C as indicated in Fig. 2. The surface fraction of spall then increases up to 3.5% at 55 cycles, while the surface fraction of cracks tends to level of around 20%. As a matter of fact, the crack network is fully completed after 20 to 40 cycles when all cells are closed and prone to easily detach from the substrate. The oblique lighting view of the specimen after 55 cycles in Fig. 1 clearly reveals the undulated morphology of the specimen surface whose occurrence is the result of

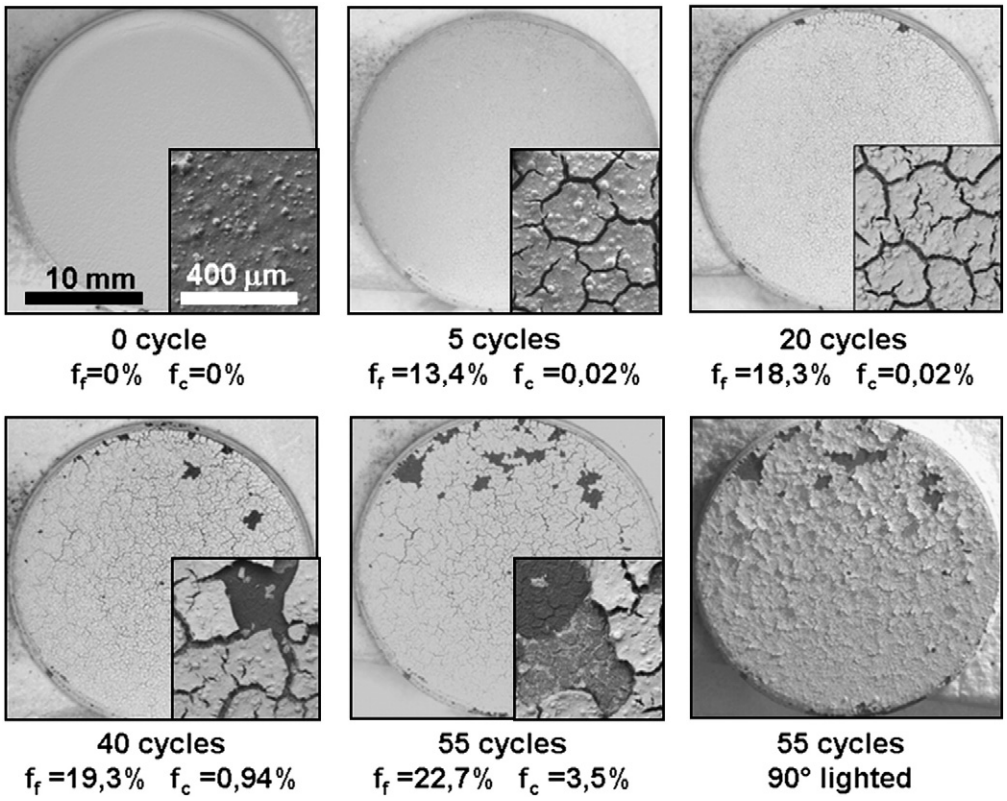

Fig. 1. Low and high magnification photographs of the surface of a sol–gel thermal barrier coating after 1 h thermal cycles at 1150 °C in laboratory air.

a partial detachment of the edges of individual cells. Differential stress release tends to strain the deposit, which deforms through bending after losing adherence to the substrate at its edges. Consequently, the surface of detached YSZ from the substrate is probably much higher than the surface of spalled YSZ determined using image analysis of photographs taken with vertical lighting. The onset of YSZ detachment from the substrate also likely occurs before the onset of YSZ spallation.

3.2. Rumpling of the bond coat

Rumpling results from the deformation of the underlying substrate subsequently to the accumulation of oxidation cycles and the associated thermal stresses. The deformation may provoke the corrugation of the thermally grown oxide (TGO) at the TBC/bond coating interface. This may cause crack initiation at the interface and propagation at the interface, in the TGO or in the YSZ [11,12]. The propensity of the substrate to develop rumpling is related to the capability of the deposit, according to its mechanical properties, to

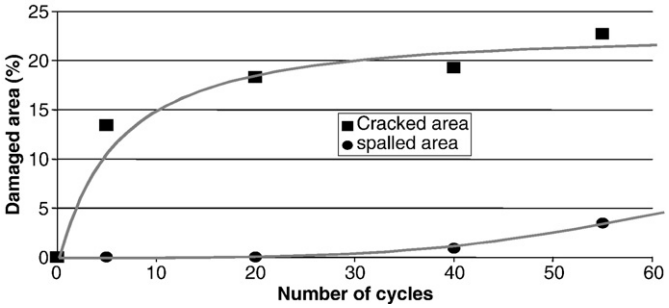

Fig. 2. Evolution of the surface fraction of cracks and spalls versus the number of 1 h oxidation cycles at 1150 °C in laboratory air.

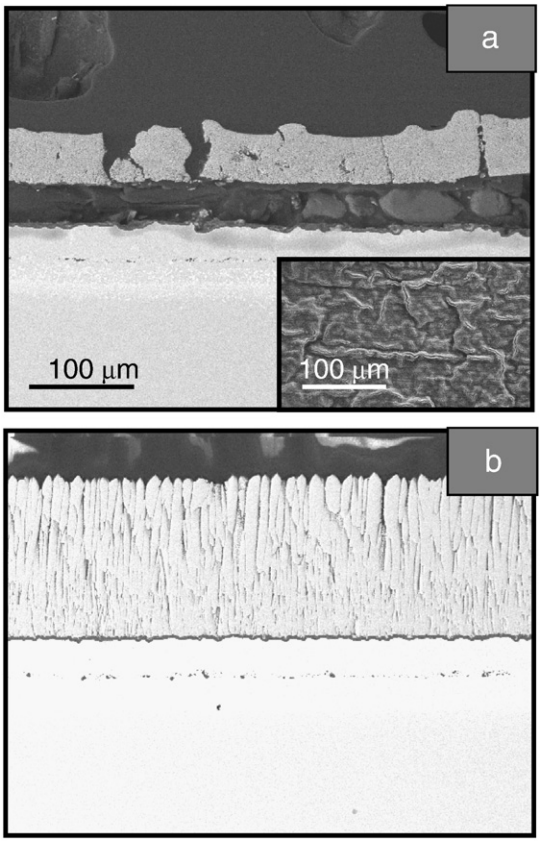

Fig. 3. Rumpling of the NiPtAl bond coat a) sol gel TBC, b) EB-PVD TBC, after 55 cycles of 1 h at 1150 °C in laboratory air.

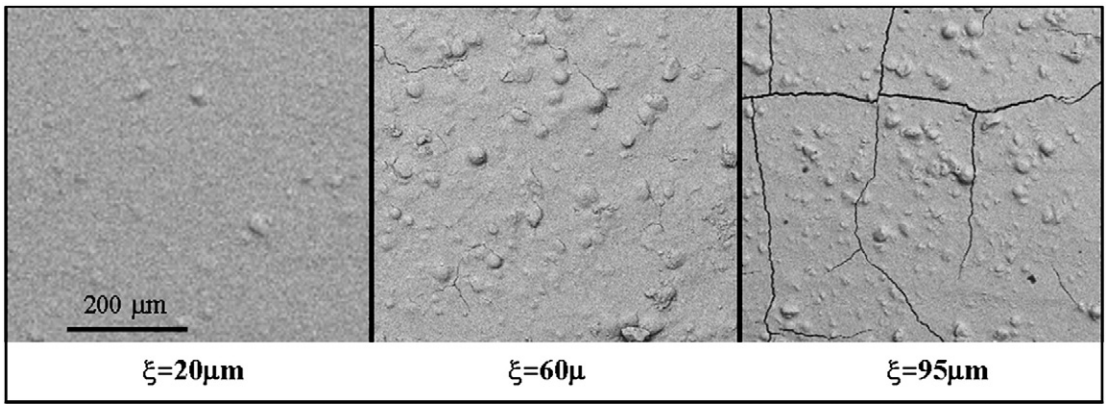

Fig. 4. Initial surface of as deposited, as heat-treated sol gel TBC versus as a function of TBC thickness (ξ).

avoid or not the establishment of plastic strain under the stress state due to thermal cycling and due to growth stresses in the TGO. Fig. 3 compares the cross-sections of a sol–gel and an EB-PVD thermal barrier coating after 55 cycles at 1150 °C. A view of the spalled surface is inserted in the cross-section image of the sol-gel TBC. Clearly, the EB-PVD TBC is still perfectly adherent as no spallation occurred after 55 cycles. In relation with this high adherence almost no rumpling is visible as far as the TBC remains in intimate contact with the substrate. On the contrary, the sol–gel TBC, largely spalled off, is characterized by high rumpling attested by both cross-section and surface imaging. The crack pattern present in the sol–gel TBC fragments the ceramic which cannot constrain the bond coat and avoid its deformation as in standard EB-PVD TBC [13]. The occurrence of more pronounced rumpling in the case of sol–gel TBC indicates the lower adherence of those barriers as compared to standard EB-PVD barriers. Note that in this case, the spallation occurs mainly at the interface between the TBC and the TGO whereas the spallation develops preferentially at the interface between the superalloy and the TGO in EB-PVD TBC. The same comparison between rumpling of EB-PVD and sol–gel TBC was already observed after cycling at 1100 °C [8].

3.3. Influence of the TBC thickness

Fig. 4 shows SEM micrographs of the initial surface after dip-coating and heat treatment for three specimens with different thicknesses ranging from 20 µm to 95 µm. The surface aspect varies significantly from the low thickness TBC, essentially smooth with no detectable crack, to the medium and high thickness TBC where cracks gradually develop. For the intermediate thickness, the process-induced cracks have slightly developed only. Cracks are localised around their initiation sites and no continuous network is formed. For thicker TBC (95 µm), cracks have propagated further and an almost continuous network of cracks has formed delineating YSZ cells about 100 to 200 µm large. It may be concluded that the effect of sintering, discussed above, leading to the formation of cracks is not effective below a critical thickness which lies between 20 µm and 60 µm.

Depending on the initial thickness, the density of associated cracks and the degree of completion of the crack network, the resistance of TBC to further cracking and spallation will differ strongly. Figs. 5 and 6 present the surface morphology of the three TBC described in Fig. 4, along with the relationship of the surface fractions of crack and spalls with the TBC thickness. For the thinnest TBC, the surface remains entirely undamaged after 55 cycles as a consequence of the uncracked initial morphology of the deposit, the surface fraction of cracks and spalls measured using image analysis are zero. For thicker TBC, cyclic oxidation results in a partial damage of the top YSZ by spallation. The surface fraction of crack is very similar for 60 µm and 95 µm thick TBC, about 23%. This corresponds accurately to the limit value of the surface fraction of cracks detailed in Fig. 2, corresponding to the full completion of the crack network prior to the occurrence of significant spallation. The surface fraction of spall differs slightly from 3.5% to 7.8%, respectively for the 60 µm and the 95 µm thick TBC. This indicates that the degradation through spallation of the TBC strongly depends on the initial thickness of the TBC while the development of the sintering induced cracks is not thickness dependent. This latter parameter is only a function of the number of cumulative cycles imposed to the specimens up to a given number of cycles, between 20 and 40, beyond which this parameter tends to stabilize around 20–25%.

3.4. Influence of the oxidation temperature

As shown previously, oxidising specimens at 1150 °C lead to a dramatic spallation of the TBC. Following 55 cycles, two mechanisms were identified, namely the establishment of a regular crack network and the detachment of individual YSZ cells. Such spallation occurs as

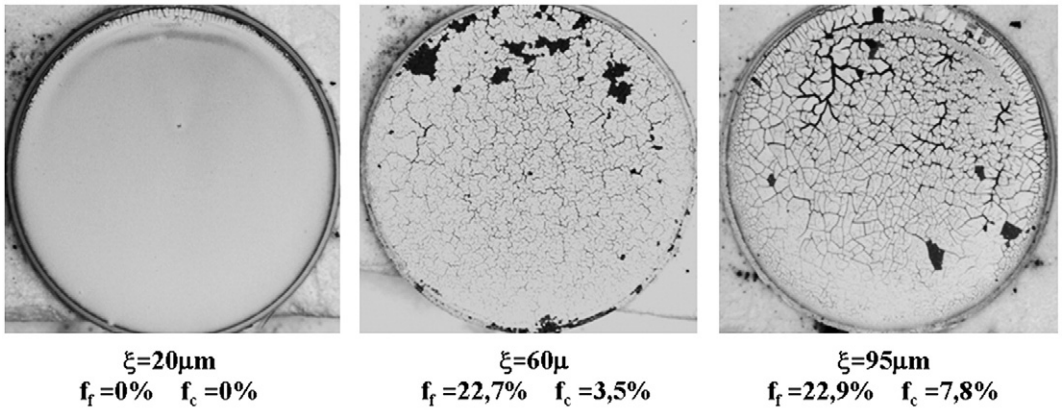

Fig. 5. TBC surface after 55 cycles of 1 h at 1150 °C as a function of TBC thickness (ξ).

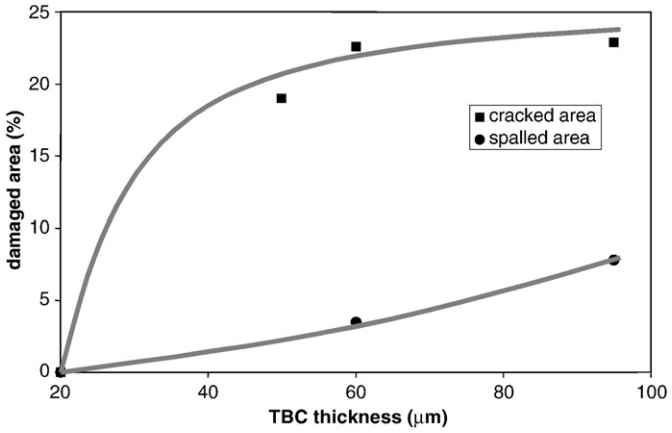

Fig. 6. Surface fraction of cracked and spalled TBC versus the thickness of the sol–gel TBC following 55 cycles of 1 h at 1150 °C.

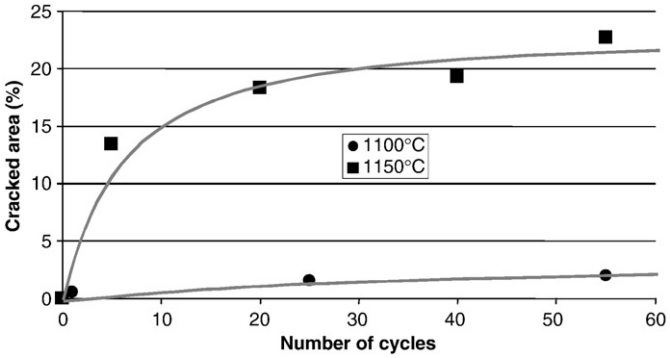

Fig. 8. Surface fraction of cracks versus the number of cycles for oxidation of 1 h at 1100 °C and 1150 °C.

the crack network has fully developed for a given number of cycles beyond which the surface fraction of spall does not increase anymore. For oxidation at lower temperature, that is 1100 °C, the onset of spallation is not reached after 55 cycles and only cracking is observed at the surface of specimens as shown in Fig. 7a. The crack network is however much less pronounced than for TBC cyclically oxidised at 1150 °C (Fig. 7b) where a dense pattern of widely opened crack is observed. At 1100 °C, the total surface fraction of cracks increases up to 3.2% which is far below the critical value identified to generate the first spalled particles, that is around 20%. As a comparison, data of Fig. 2, indicating the surface fraction of crack for the specimen oxidised at 1150 °C versus the number of cycles, are plotted in Fig. 8. Whereas the TBC oxidised at 1150 °C exhibits the threshold surface fraction of cracks after 20 to 40 cycles, the TBC oxidised at 1100 °C is unspalled at this stage and the surface fraction of crack is still very low. Providing mechanisms remain unchanged, a simple linear extrapolation of data obtained at 1100 °C gives an estimated number of cycles to reach a surface fraction of cracks of about 20% close to 350 to 400. This would be the number of cycles required for the onset of spallation, which can be related with previous work showing only little degradation for similar sol–gel TBC after 500 cycles [8].

4. Conclusion

By optimizing the sol formulation, it has been possible to obtain homogeneous YSZ thermal barrier coatings by sol–gel route. The microstructure of the deposit has been adjusted to have a good recovering of the substrates. The obtained coating, with various controlled achievable thicknesses, shows an equiaxe microstructure with very little porosity.

In as deposited TBC, the outer surface is satisfactorily homogeneous as a consequence of the optimisation of the manufacturing process.

After few oxidation cycles, a crack network is observed resulting from the sintering of the YSZ grains. Compared to the conventional EBPVD and Plasma Spray coatings, this confers to the sol–gel systems a specific degradation mode corresponding to the heat checking of the TBC. The crack density rapidly increases with the first oxidation cycles and consequently the size of cells delineated by the cracks decreases. Beyond a certain number of cycles, circa? 20 to 30, the crack density reaches a threshold value. This determines the onset for spallation as cells start to individually detach from the substrate. On the contrary to what is usually observed in EB-PVD TBC systems with the same superalloy and bondcoating, where decohesion occurs at the metal/TGO interface, spallation of sol–gel TBC occurs preferentially at the TGO/TBC interface. After 55 cycles at 1100 °C, very little heat checking occurred and no spallation was noted. After 55 cycles at 1150 °C, spallation remains moderate, namely lower than 25%. As a matter of fact, the development of the crack network and the propensity to spallation are enhanced as the sol–gel YSZ thickness is increased. As a result of the mechanical properties of the sol–gel coatings, the bond coat rumpling is more pronounced in sol–gel TBC than in standard EB-PVD TBC.

Though the number of oxidation cycles imposed in this study has been moderate, the behaviour of sol–gel TBC is promising as the resistance to spallation is satisfactory either at 1100 °C or at 1150 °C. In addition, sol–gel processing can be quite easily implemented and

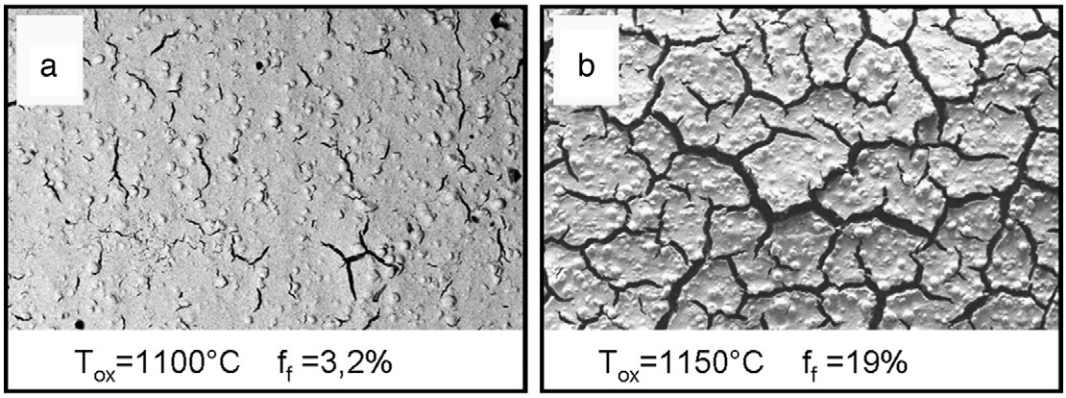

Fig. 7. Influence of the oxidation temperature on the surface fraction of crack for 50 μm thick sol–gel TBC on the morphology and extent of the crack network after 55 × 1 h cycles.

may be considered as a great potential route to either manufacture or repair thermal barrier coatings.

Acknowledgements

Authors gratefully acknowledge the financial support of the French Research Agency (ANR) under contract CISBAT.

References

[1] C. Viazzi, J.-P. Bonino, F. Ansart, A. Barnabé, J. Alloys Compd. 452 (2) (March 20 2008) 377.
[2] C. Viazzi, J.P. Bonino, F. Ansart, Surf. Coat. Technol. 201 (7) (December 20 2006) 3889.
[3] J. Fenech, C. Viazzi, J.-P. Bonino, F. Ansart, A. Barnabé, Ceram. Int. 35 (8) (December 2009) 3427.
[4] C. Viazzi, R. Wellman, D. Oquab, J. Nicholls, D. Monceau, J.P. Bonino, F. Ansart, Mater. Sci. Forum 595–598 (2008) 3.
[5] Barrow et al, US patent n° 005585136A, (1996).
[6] C.R. Xia, et al., Solid State Ionics 133 (2000) 287.
[7] D. Monceau, F. Crabos, A. Malié, B. Pieraggi, Mater. Sci. Forum 5 (2001) 607.
[8] V. Menvie Bekale, D.Monceau, D.Oquab, Florence Ansar, J.P. Bonino, Actes conférence Eurocorr, 6-10 Septembre 2009, Nice (2009).
[9] J. Sniezewski, Y. Le Maoult, P. Lours, Mater. High Temp. 27 (2) (2010) 101.
[10] M. Madhwal, E. Jordan, M. Gell, Mat. Sci & Eng. A 384 (2004) 151.
[11] A.G. Evans, D.R. Mumm, J.W. Hutchinson, G.H. Meier, F.S. Pettit, Mater. Sci. 46 (5) (2001) 505.
[12] D.S. Balint, J.W. Hutchinson, J. Mech. Phys. Solids 53 (4) (April 2005) 949.
[13] V.K. Tolpygo, D.R. Clarke, K.S. Murphy, Surf. Coat. Technol. 188–189 (2004) 62.